Coulombic and radiative decay rates of the resonances of the exotic molecular ions $pp\mu$, $pp\pi$, $dd\mu$, $dd\pi$, and $dt\mu$

Senem Kilic,[1,2] Jean-Philippe Karr,[1,2] and Laurent Hilico[1,2,*]

[1]*Laboratoire Kastler Brossel, Université Pierre et Marie Curie T12, Case 74, 4 place Jussieu, 75252 Paris, France*
[2]*Département de Physique et Modélisation, Université d'Evry Val d'Essonne, Boulevard F. Mitterrand, 91025 Evry cedex, France*

The bound levels and the resonances (energy and width of the excited levels) of $pp\mu$-like exotic molecules for $J=0$ total angular momentum have been computed with an accuracy in the 10^{-11} a.u. range, by numerical diagonalization of the complex rotated Hamiltonian in a variational sturmian basis set. For the resonances below the $N=2$ dissociation threshold, the x-ray spontaneous emission spectrum is computed from the wave functions. The radiative decay rate of the first resonance of $pp\mu$ is found to be 0.0713 ps^{-1}, close to half that of a $p\mu(2p)$ atom, as expected in a simple Born-Oppenheimer picture of a resonance.

I. INTRODUCTION

Recently, spectroscopy experiments on exotic atoms such as $p\mu$ [1] have been performed at the Paul Scherrer Institute (PSI). The exotic atoms are produced by sending muons in a dense molecular hydrogen target. They are produced in very excited states ($N \approx 14$) and then rapidly decay down to the ground $1s$ state or the metastable $2s$ state. Of particular interest is the metastable $2s$ state from which the $2s$-$2p$ muonic Lamb shift could be measured [2]. Such an experiment is only feasible if the $p\mu(2s)$ population is large enough. Recently, evidence for the production of $p\mu(2s)$ states has been obtained and interpreted [1,3] as follows.

The $2s$ states have most probably been observed indirectly through a quenching mecanism that involves the $pp\mu$ resonances (excited states below the $N=2$ dissociation threshold). It results in the formation of high kinetic energy (≈ 900 eV) $p\mu(1s)$ atoms. Indeed, resonant collision between $p\mu(2s)$ atoms and H_2 leads to the formation of $pp\mu$ excited muonic molecules. The Coulomb decay of those resonances lying ≈ 1800 eV above the $N=1$ dissociation threshold may produce $p\mu(1s)$ atoms with a kinetic energy in the 900 eV range, corresponding to the narrow high energy component observed on the kinetic energy distribution of $p\mu(1s)$ atoms in the PSI experiment.

In addition to the direct Coulomb decay channel $pp\mu^* \rightarrow p\mu(1s)+p$, the excited states of the muonic molecules can dissociate through the radiative channel $pp\mu^* \rightarrow p\mu+p+\gamma$. In that case, most of the energy is taken by the photon so the $p\mu$ atom and the proton only acquire a small kinetic energy. For $pp\mu$ molecules, the Coulomb decay channel is much faster than the radiative one, the branching ratio to the Coulomb channel being more than 97% [4]. This explains why the quenching mecanism described above can be observed on the kinetic energy distribution of the $p\mu(1s)$ atoms. In the case where H_2 is substitued by D_2, the $d\mu(2s)$ quenching mecanism involves excited $dd\mu$ molecules. The Coulomb

decay rate of the $dd\mu$ resonances is slower than that of $pp\mu$ by two orders of magnitude whereas the radiative decay rates are comparable. As a consequence, the branching ratio to the Coulomb decay channel decreases to a few percent, as was first noticed by Lindroth [4]. As a consequence, only a small amount of high kinetic energy $d\mu$ atoms is expected, as was verified experimentally.

Pionic hydrogen spectroscopy experiments are also conducted at PSI [5,6] to determine the strong interaction shift and absorption width of the $p\pi(1s)$ level from the $(Np) \rightarrow (1s)$ lines, $N=2$, 3 or 4. Those $p\pi$ atoms are produced from higly excited atoms through an atomic cascade during which $pp\pi$ resonances can be populated. The knowledge of the spectral properties of those resonances is important to know if they can affect the measured $p\pi$ line position and shape. Indeed, radiative decay from a $pp\pi$ resonance bound by a few eV below the $p\pi(N)$ dissociation limit may shift down the x-ray line position. In other respects, Coulomb decay of $pp\pi$ resonances is one of the efficient processes leading to high kinetic energy $p\pi$ atoms that contributes to Doppler broadening of the $p\pi$ lines [6–8]. Of course, the Coulomb and radiative rates of the $pp\pi$ resonances have to be compared to the nuclear absorption rate.

In Sec. II, we present the full three-body calculation of the $^1S^e$ and $^{1,3}P^o$ bound levels and $^1S^e$ resonance complex energies for the $pp\mu$, $dd\mu$, $pp\pi$, $dd\pi$, and $dt\mu$ molecular ions below the $N=2$ dissociation limit. The knowledge of the $dt\mu$ resonances energies and widths is useful for the evaluation of their impact in the muon catalyzed fusion cycle [9]. Both the resonance energies and widths obtained from the imaginary part of the complex energy are given. The accuracy of our results is improved by several orders of magnitude as compared to previously published ones. We also discuss the structure of the spectrum of resonances and of the wave functions, and show that although the muon to proton (or deuteron) mass ratio is less than 10, the real part of the energy of the resonances is consistent with a simple Born-Oppenheimer (BO) picture. Of course, the widths of the resonances are zero in the standard BO approximation, hence the nonzero widths we obtained are a direct measure of the breaking of the BO approximation.

*Electronic address: hilico@spectro.jussieu.fr
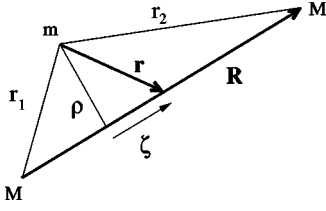
FIG. 1. The radial coordinates (R, ρ, ζ) in the three body plane.

In Sec. III, we present the calculation of the x-ray emission spectrum of the $^1S^e$ resonances and obtain their radiative decay rates as well as the branching ratios between the Coulomb and radiative decay channels.

II. BOUND AND RESONANT STATES

A. Structure of the wave functions

The energy levels and the corresponding wave functions of the Schrödinger three body problem are labeled by the quantum numbers (J, M_J) related to the total angular momentum and by their discrete symmetries, the parity Π and the exchange of the two nuclei P_{12}. In [10], we have presented in detail the structure of the $J=0$ and $J=1$ wave functions, and the Schrödinger equation they obey. In this section, we recall the essential points of this formalism in the case of homonuclear ions and apply them to the exotic molecular ions. We will use atomic units related to the lightest particle, the muon or the pion. M/m is the ratio of the nucleus to the light particle mass. a_0 is the muonic or pionic Bohr radius.

The centered Jacobi coordinates $\mathbf{R}$ and $\mathbf{r}$ depicted in Fig. 1 represent the relative position of the two nuclei and that of their center of mass with respect to the lightest particle. The quantities $\mathbf{P}$ and $\mathbf{p}$ are the conjugate momenta, so the Hamiltonian writes

$$H = \frac{q^2}{4\pi\epsilon_0 a_0}\left[\frac{\mathbf{p}^2}{2} + \frac{M}{m}\left(\mathbf{P}^2 + \frac{\mathbf{p}^2}{4}\right) - \frac{1}{\|\mathbf{R}/2 - \mathbf{r}\|}\right.$$
$$\left. - \frac{1}{\|\mathbf{R}/2 + \mathbf{r}\|} + \frac{1}{R}\right]. \tag{1}$$

To represent the dimensionless quantities $\mathbf{R}$ and $\mathbf{r}$, we use the three Euler angles (θ, Ψ, ϕ) and two sets of radial coordinates (see Fig. 1 in Ref. [11]). The first one is (R, ρ, ζ) where ζ is the projection of $\mathbf{r}$ on the direction of $\mathbf{R}$ and $\rho = \sqrt{r^2 - \zeta^2}$. The second one is the perimetric coordinate set [12] defined from the three interparticle distances by

$$x = r_1 + r_2 - R,$$

$$y = r_1 - r_2 + R,$$

$$z = -r_1 + r_2 + R.$$

For the $^{1,3}S^e$ ($J=0$, $M_J=0$, $\Pi=1$, $P_{12}=\pm 1$) states, the angular part of the wave function is isotropic ($\mathcal{D}^0_{0\,0} = 1/\sqrt{8\pi^2}$), so we write the wave function as

$$\Psi^{J=0, M_J=0}(\mathbf{R}, \mathbf{r}) = \frac{1}{\sqrt{8\pi^2}}\Phi(x, y, z). \tag{2}$$

The radial function Φ verifies $\Phi(x, z, y) = \pm\Phi(x, y, z)$ for symmetric or antisymmetric states ($P_{12} = \pm 1$). The $^1P^o$ states ($J=1$, $\Pi=-1$, $P_{12}=1$) and the $^3P^o$ states ($P_{12}=-1$) can be factored out using two orthogonal angular functions and only one radial function $F_{M_J}(x, y, z)$ as

$$\Psi^{J=1, M_J}(\mathbf{R}, \mathbf{r}) = \mathcal{D}^{1*}_{M_J 0}(\theta, \psi, \phi)\left[\left(\zeta + \frac{1}{2}R\right)F_{M_J}(x, y, z)\right.$$
$$\left. \pm \left(\zeta - \frac{1}{2}R\right)F_{M_J}(x, z, y)\right]$$
$$+ \frac{\mathcal{D}^{1*}_{M_J-1}(\theta, \psi, \phi) - \mathcal{D}^{1*}_{M_J 1}(\theta, \psi, \phi)}{\sqrt{2}}$$
$$\times \rho[F_{M_J}(x, y, z) \pm F_{M_J}(x, z, y)],$$

where the $\mathcal{D}^J_{M_J T}$ functions are the matrix elements of the rotation operator mutiplied by a factor $\sqrt{(2J+1)/8\pi^2}$. The effective Schrödinger equation satisfied by the radial functions Φ (for the $^{1,3}S^e$ states) and F_{M_J} (for the $^{1,3}P^o$ states) is a generalized eigenvalue problem for the energy E that takes the form

$$A|\Phi\rangle = EB|\Phi\rangle. \tag{3}$$

B. Numerical implementation

1. The bound states

The linear problem (3) is solved for the bound states of the molecular ions by expanding the wave function on the Sturmian basis set defined by

$$|n_x^\alpha, n_y^\beta, n_z^\beta\rangle = |n_x^\alpha\rangle \otimes |n_y^\beta\rangle \otimes |n_z^\beta\rangle, \tag{4}$$

where $|n_u^\alpha\rangle$ represents the function

$$\Phi_n(\alpha u) = \langle u|n^\alpha\rangle = (-1)^n\sqrt{\alpha}L_n^{(0)}(\alpha u)e^{-\alpha u/2}, \tag{5}$$

and where $L_n^{(0)}$ is a Laguerre polynomial. n is a non-negative integer, α^{-1} is the length scale in the x direction, β^{-1} in the y and z directions. The matrices representing the operators A and B are real and symmetric sparse banded matrices, where all matrix elements are known in analytic form [10]. The generalized eigenvalue problem (3) is then solved using the Lanczos algorithm that gives the eigenvalues in the energy range of interest as well as the corresponding eigenvectors. Because of the numerical truncation of the basis ($n_x \leq N_{x_{max}}$ and $n_x + n_y + n_z \leq N_{base}$), the length scales α^{-1} and β^{-1} become variational parameters. They are optimized to stabilize the eigenenergies. Table I presents the $J=0$ and $J=1$ bound states of $pp\mu$, $dd\mu$, $pp\pi$ and $dd\pi$ as well as those of $dt\mu$. For the symmetric molecular ions, the mass ratios $m_p/m_\mu = 8.88024408$ and $m_d/m_\mu = 17.75167454$ are those given by the 1999 CODATA [13]. The proton (and deuteron) to pion mass ratios are obtained from [15] and are $m_p/m_\pi = 6.7225821$, $m_d/m_\pi = 13.4384920$. The muonic atomic en-

TABLE I. Bound states energies of the exotic molecular ions in (muonic or pionic) atomic units and corresponding binding energies in eV. v is the vibrational quantum number. The dissociation limits are obtained from the mass ratios by $E_{diss}(N)=-(1/2N^2)[1/(1+M/m)]$. See text for the values of the relevant mass ratios.

	v	Energy (a.u.)	Binding energy (eV)
		$pp\mu$	
$^1S^e$	0	−0.494 386 817 912	253.150 075
$^3P^o$	0	−0.468 458 433 545	107.265 302
		−0.449 393 962 745	diss. lim. N=1
		$dd\mu$	
$^1S^e$	0	−0.531 111 133 962	325.070 540
	1	−0.479 706 378 902	35.844 227
$^3P^o$	0	−0.513 623 954 981	226.679 792
	1	−0.473 686 732 637	1.974 985
		−0.473 335 714 685	diss. lim. N=1
		$pp\pi$	
$^1S^e$	0	−0.474 927 514 376	294.859 440
$^3P^o$	0	−0.446 049 252 053	80.227 499
		−0.435 254 815 873	diss. lim. N=1
		$dd\pi$	
$^1S^e$	0	−0.518 153 620 861	392.301 199
	1	−0.467 493 120 397	15.777 106
$^3P^o$	0	−0.497 298 725 502	237.301 338
		−0.465 370 344 873	diss. lim. N=1
		$dt\mu$	
S^e	0	−0.538 594 975 061	319.136 818
	1	−0.488 065 357 852	34.834 430
P^o	0	−0.523 191 456 316	232.469 683
	1	−0.481 991 529 974	0.660 338
		−0.481 874 166 748	$t\mu$ diss. lim. N=1

ergy unit is 5626.450561 eV, and the pionic one is 7432.301093 eV. For the $dt\mu$ calculations, we have used the mass ratios of the 1986 CODATA [14] $m_\mu/m_e=206.768262$, $m_d/m_e=3670.483014$ and $m_t/m_e=5496.92158$. Because of the slighlty different muon mass, the muonic atomic energy unit is 5626.450461 eV in the case of $dt\mu$.

In the case of $dd\mu$ and $dt\mu$, we obtain two P^o levels, the excited one ($v=1$) being very sligtly bound by 1.97 eV or 0.66 eV. We have searched that level for $dd\pi$ by varying the basis size as well as α and β. Even though the muon and pion mass only differ by 25%, we can conclude that most probably the $v=1$ $^3P^o$ level of $dd\pi$ does not exist, and thus that we have obtained all the S^e and P^o bound levels of the molecular ions.

In Table II, we compare the $^1S^e$ and $^3P^o$ bound states of $pp\mu$ computed using our method in FORTRAN double precision to the results given by Bailey and Frolov [16] at the 10^{-19} a.u. accuracy level. The results are in perfect agreement. In the case of $dt\mu$, our results compare well with those given by other groups [16–19].

TABLE II. Comparison of the $v=0$ resonance of $pp\mu$ given by Bailey and Frolov. For those calculations, we have used $m_p/m_\mu=8.880\ 244\ 401\ 338\ 54$.

	Energy (a.u.)	
$^1S^e$	−0.494 386 820 248 934 791 1	[19]
	−0.494 386 820 248 92	This work
$^3P^o$	−0.468 458 436 303 384 803	[19]
	−0.468 458 436 303 38	This work

2. The resonances

In the frame of the Born-Oppenheimer approximation, the bound levels of the molecular ions are supported by the first $1s\sigma_g$ electronic energy curve. Figure 2 shows the BO curves converging to the successive $N=1$, 2 and 3 dissociation thresholds of the molecular ion. They are labelled using the usual molecular terms and we have indicated the exact symmetries of the S^e and P^o resonances they support. In the lowest order BO approximation, the various electronic energy curves are not coupled and the resonances appear as bound levels. In our calculations, the three body dynamics are fully taken into account, i.e., all the couplings between BO curves are considered. Those couplings turn the discrete excited states into resonances of finite lifetime.

From the numerical point of vue, the resonances supported by an excited electronic state of the molecular ion are embedded in the continua of the lower electronic states. They can be separated by using the complex dilation method [20]. It consists in multiplying the radial coordinates, and thus the
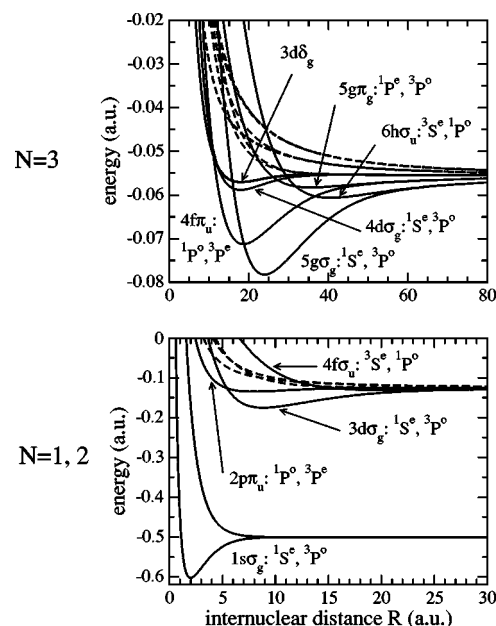
FIG. 2. Born-Oppenheimer electronic energy curves below the $N=2$ and $N=3$ thresholds. The binding curves are plotted with solid lines. They are labeled by the usual molecular quantum numbers. We also indicate the exact symmetries of the $^{1,3}S^e$ and $^{1,3}P^o$ resonances they support. The $3d\delta_g$ curve only supports states of total angular momentum greater than 2.

TABLE III. $^1S^e$ resonances of $pp\mu$, $dd\mu$, and $dt\mu$ under the $N=2$ threshold. The real and imaginary parts of the complex energies are in muonic atomic units. The corresponding binding energies and Coulomb width are in eV and meV. Γ_C and Γ_γ are the Coulombic and radiative decay rates. $\Upsilon_\gamma = \Gamma_\gamma/(\Gamma_c + \Gamma_\gamma)$ is the branching ratio between the two decay channels. The resonances below the $N=2$ (respectively $N=3$) threshold that are labeled by a vibrational number v are supported by the $3d\sigma_g$ (respectively $5g\sigma_g$) BO curves. Numbers in brackets denote powers of 10.

v	Re(E) (a.u.)	E_b (eV)	Im(E) (a.u.)	$\hbar\Gamma_c/2$	Γ_c	Γ_γ	Υ_γ
$pp\mu$				(meV)	(ps)$^{-1}$	(ps)$^{-1}$	
0	−0.146 404 680 88	191.615 470	1.513[−7]	0.851	2.587	0.0713	0.027
1	−0.128 885 489 08	93.044 604	2.625[−7]	1.477	4.487	0.0609	0.013
2	−0.118 028 794 48	31.959 948	2.062[−7]	1.160	3.526	0.0569	0.016
3	−0.113 949 703 23	9.009 143	6.157[−8]	0.346	1.053	0.0571	0.051
4	−0.112 844 246 53	2.789 346	1.943[−8]	0.109	0.332	0.056	0.144
5	−0.112 504 563 6	0.878 137	6.15[−9]	0.035	0.105		
	−0.112 348 490 69		dissociation limit $N=2$				
$dd\mu$				(μeV)	(ps)$^{-1}$	(ps)$^{-1}$	
0	−0.157 099 321 63	218.111 567	3.411[−10]	1.919	0.0058	0.0804	0.932
1	−0.142 377 329 00	135.279 003	1.031[−9]	5.801	0.0176	0.0708	0.801
2	−0.131 302 505 83	72.967 058	1.630[−9]	9.171	0.0279	0.0648	0.699
3	−0.124 003 892 20	31.901 769	1.453[−9]	8.175	0.0248	0.0621	0.714
4	−0.120 576 317 12	12.616 688	6.674[−10]	3.755	0.0114	0.0619	0.844
5	−0.119 277 925 05	5.311 349	2.914[−10]	1.640	0.0050		
6	−0.118 738 317 42	2.275 273	1.27[−10]	0.715	0.0022		
7	−0.118 508 324 99	0.981 232	5.5[−11]	0.309	0.0009		
	−0.118 333 928 67		dissociation limit $N=2$				
$dt\mu$				(μeV)	(ps)$^{-1}$	(ps)$^{-1}$	
0	−0.159 194 524 79	217.889 825	1.742[−10]	0.98	0.0030	0.0731	0.96
1	−0.145 303 272 20	139.731 381	4.217[−10]	2.373	0.0072	0.0729	0.91
2	−0.134 531 308 61	79.123 461	5.798[−10]	3.262	0.0099	0.0638	0.87
3	−0.126 977 943 64	36.624 828	5.053[−10]	2.843	0.0086	0.0630	0.88
4	−0.123 573 012 24	17.467 150	1.421[−10]	0.800	0.0024	0.0601	0.96
5	−0.122 499 264 57	11.425 762	5.879[−11]	0.331	0.0010		
6	−0.121 758 063 06	7.255 428	1.43[−10]	0.805	0.0024		
7	−0.121 104 831 12	3.580 051	5[−11]	0.281	0.0009		
	−0.120 468 541 69		$t\mu$ dissociation limit, $N=2$				
				(meV)	(ps)$^{-1}$		
0	−0.119 224 582 64	5.011 219	1.123[−4]	632	1920		
1	−0.118 748 636	2.333 3	5.593[−5]	315	956		
2	−0.118 53	1.1	3[−5]	169	513		
	−0.118 333 928 88		$d\mu$ dissociation limit, $N=2$				

perimetric coordinates by $e^{i\theta}$. The complex dilation method is straightforward to implement from the bound state calculation since it simply consists in turning the inverse length scales α and β into $\alpha e^{-i\theta}$ and $\beta e^{-i\theta}$ in the definition of the basis functions (5). The matrices A and B become non-Hermitian complex symmetric sparse banded matrices. Numerically, we observe the well known properties of the complex dilation method. The bound levels are unchanged, being the real eigenvalues of the problem. The continuous spectrum is rotated out in the complex plane by an angle 2θ around the consecutive thresholds. Provided the rotation angle is large enough to uncover the resonances, they appear

as stationary complex eigenvalues of the Schrödinger equation. The real and imaginary parts give the energy E_r and Coulomb width Γ_{Coul} of the resonances, i.e.,

$$E_{res} = E_r - \frac{i}{2}\Gamma_{Coul}. \qquad (6)$$

Tables III and IV present the S^e complex energies of $pp\mu$, $dd\mu$, $pp\pi$, $dd\pi$, and $dt\mu$, in atomic units and also in eV. The convergence of the complex energies is obtained for rather large domains in the variational space. For $N_{base}=92$ and $N_{x_{max}}=20$, the $^1S^e$ basis for homonuclear ions contains 37234

TABLE IV. The same as Table III but for $pp\pi$ and $dd\pi$, under the $N=2$, 3 and 4 dissociation thresholds. Numbers in brackets denote powers of 10.

v	Re(E) (a.u.)	E_b (eV)	Im(E) (a.u.)	$\hbar\Gamma_c/2$	Γ_c	Γ_γ	Υ_γ
$pp\pi$				(meV)	(ps)$^{-1}$	(ps)$^{-1}$	
0	−0.140 590 327 83	236.173 436	1.993[−7]	1.481	4.501	0.0879	0.019
1	−0.122 288 143 62	100.146 093	2.588[−7]	1.923	5.845	0.0745	0.013
2	−0.112 395 810 61	26.623 295	1.285[−7]	0.955	2.902	0.0716	0.024
3	−0.109 723 714 44	6.763 472	3.077[−8]	0.229	0.695		
4	−0.109 058 741 50	1.821 193	8.266[−9]	0.061	0.187		
	−0.108 813 703 97		dissociation limit $N=2$				
0	−0.064 343 477 84	118.781 785	8.249[−7]	6.131	18.63		
1	−0.057 884 439 37	70.776 266	1.402[−6]	10.42	31.66		
2	−0.053 193 463 30	35.911 519	1.363[−6]	10.13	30.78		
3	−0.050 529 763 27	16.114 099	7.422[−7]	5.516	16.76		
4	−0.049 372 872 61	7.515 739	3.72[−7]	2.765	8.40		
	−0.049 099 229 97	5.481 945	1.121[−6]	8.332	25.32		
	−0.048 361 646 21		dissociation limit $N=3$				
0	−0.036 370 450 93	68.132 089	2.601[−6]	19.33	58.74		
1	−0.033 476 493 39	46.623 326	5.210[−6]	38.72	117.7		
	−0.031 427	31.39	3.28[−6]	24.4	74.1		
	−0.031 139 889 80	29.256 984	6.227[−6]	46.28	140.6		
	−0.029 484 517 12	16.953 756	5.267[−6]	39.15	118.9		
	−0.027 203 425 99		dissociation limit $N=4$				
$dd\pi$				(μeV)	(ps)$^{-1}$	(ps)$^{-1}$	
0	−0.153 380 951 59	275.280 283	6.679[−9]	49.64	0.1508	0.1023	0.404
1	−0.137 442 615 99	156.821 774	1.299[−8]	96.546	0.2933	0.0887	0.232
2	−0.126 156 476 60	72.939 788	1.374[−8]	102.12	0.3103	0.0812	0.207
3	−0.119 853 579 63	26.094 760	7.291[−9]	54.189	0.1647	0.0795	0.326
4	−0.117 619 574 60	9.490 962	2.597[−9]	19.302	0.0586		
5	−0.116 826 878 60	3.599 407	9.91[−10]	7.365	0.0224		
6	−0.116 528 288 78	1.380 197	3.81[−10]	2.832	0.0086		
	−0.116 342 586 22		dissociation limit $N=2$				
				(meV)	(ps)$^{-1}$		
0	−0.069 812 728 24	134.561 158	5.112[−8]	0.380	1.154		
1	−0.064 423 052 48	94.503 465	1.375[−7]	1.022	3.105		
2	−0.060 015 896 48	61.748 155	2.173[−7]	1.615	4.907		
3	−0.056 643 259 48	36.681 701	2.388[−7]	1.775	5.393		
4	−0.054 448 729 54	20.371 294	1.757[−7]	1.306	3.968		
5	−0.053 253 062 55	11.484 737	1.069[−7]	0.795	2.414		
6	−0.052 590 753 3	6.562 255	6.514[−8]	0.484	1.471		
7	−0.052 215 555 4	3.773 671	3.85[−8]	0.286	0.869		
8	−0.052 000 617 5	2.176 188	2.26[−8]	0.168	0.510		
	−0.051 707 816 10		dissociation limit $N=3$				
0	−0.039 318 541 03	76.053 953	8.916[−8]	0.663	2.014		
1	−0.036 955 341 63	58.489 943	2.145[−7]	1.594	4.843		
	−0.034 901 809 23	43.227 472	3.222[−7]	2.395	7.276		
	−0.034 056 722 42	36.946 533	3.476[−7]	2.583	7.850		
	−0.033 174 920 41	30.392 715	3.789[−7]	2.816	8.557		
	−0.029 085 646 55		dissociation limit $N=4$				

vectors. The domain is bounded by $0.5 \leqslant \alpha \leqslant 1.3$, $0.3 \leqslant \beta \leqslant 1.5$, the higher excited states being obtained near the lower bound of the domain. The rotation angle is of the order of 0.2. All the results presented here are well converged and have been rounded at the 10^{-11} a.u. level, improving the ac-

curacy of the previously published results by several orders of magnitude [3,4,8,21,22]. In the case of $dt\mu$, our resonance energies are in agreement with those given by Hara [21]. Tolstikhin [23] and Mil'nikov [24] have recently published $J=0$ resonance complex energies of $dt\mu$ below the $n=2$

TABLE V. List of the binding Born-Oppenheimer energy curves converging to the dissociation limit N. A is the static atomic dipole. δ is defined by Eq. (7) and is evaluated in the case of $^1S^e$ $pp\mu$ resonances. The theoretical values of δ compare well with the numerical ones fitted from the binding energies of Table III.

N		A	δ	Fitted δ
1	$1s\sigma_g$	0		
	$2p\pi_u$	0		
2	$2p\pi_u$	0		
	$3d\sigma_g$	3	1.223	1.196
	$4f\sigma_u$	3	1.223	
3	$3d\delta_g$	0		
	$4f\pi_u$	9/2	0.997	
	$4d\sigma_g$	0		
	$5g\pi_g$	9/2	0.997	
	$5g\sigma_g$	9	0.704	0.674
	$6h\sigma_u$	9	0.704	

threshold, pointing out large discrepancies on the width of the resonances as compared to previous results. The present work confirms, with an improved accuracy, the resonance widths they obtained (the quantities to be compared are $2\text{Im}(E)$ from Table III and the width denoted $10^9\Gamma$ in [23–25]).

3. Structure of the resonance spectrum

The structure of the resonance spectrum we have obtained can be qualitatively understood in the frame of the Born-Oppenheimer approximation, even though the proton to muon (or pion) mass ratio is not much greater than one. More precisely, we now show that the structure of the resonance spectrum is consistent with the simple picture where a resonance level below the N dissociation threshold appears as a $p\mu$ atom of principal quantum number N polarized by the field of the second nucleus. In that case, the long range behavior of the BO curves is given by $-A/R^2$, assuming the static atomic dipole A is not zero. The spectral properties of this kind of potential are discussed in [26,27] and one can show that if $\gamma \leq \frac{1}{2}$ there is no bound state and that otherwise the binding energies follow an exponential decay law given by

$$E_v^b = E_0^b e^{-2\pi v/\sqrt{\gamma^2 - 1/4}} = E_0^b e^{-\delta v}, \qquad (7)$$

where $\gamma^2 = 2\mathcal{M}A$, $\mathcal{M}$ being the reduced mass of the two nuclei in units of the light particle. The same exponential law also stands for the widths [28,29]. If $A=0$, the electronic energy curve varies as $1/R^4$ for large R, and there is only a finite number of levels. Table V gives the long range properties of the binding BO curves and compares the δ factor defined by Eq. (7) in the case of $pp\mu$ with the δ values fitted from the $pp\mu$ resonance positions given in Table III.

The binding energies of the $^1S^e$ resonances below the $N=2$ dissociation limit given in Table III for $pp\mu$ and $dd\mu$ are plotted in Fig. 3. They decrease exponentially with the vibrational quantum number v as expected in the BO model. In-
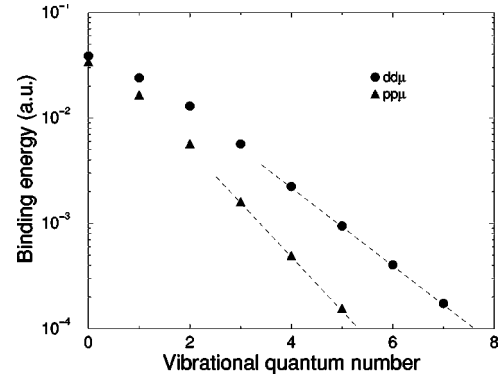
FIG. 3. Binding energies of the resonances of $pp\mu$ (triangles) and $dd\mu$ (squares) below the $N=2$ dissociation limit versus the vibrational quantum number v. The logarithmic vertical scale shows the exponential decrease of the binding energies with v.

deed, those $^1S^e$ resonances are supported by the $3d\sigma_g$ BO curve that has a static dipole $A=3$. Fitting the curves of Fig. 3 for $v \geq 3$, we obtain the decay factors 1.196 for $pp\mu$ and 0.851 for $dd\mu$, in good agreement with the values 1.223 and 0.863 predicted from Eq. (7).

The couplings with the continua result in a finite lifetime related to the width of the resonances given by the complex dilation method. When the proton is replaced by a deuteron in the molecular ions, the physical situation gets much closer to the BO approximation. As a consequence, the width of the $^1S^e$ resonances below the $N=2$ threshold dramatically decreases by 2 or 3 orders of magnitude as can be seen in Tables III and IV. One can notice that the lifetime of the muon (2.2 μs) and of the charged pion (26 ns) correspond to widths of respectively 3×10^{-14} and 1.7×10^{-12} a.u., smaller than the Coulomb widths we have obtained.

In the case of $dt\mu$, each dissociation limit is splitted in two parts, the lower corresponding to a $t\mu$ atom and the higher to a $d\mu$ atom. The resonances lying between the two dissociation limits have very large widths of the order of 1 eV. For such a level, the binding energy to the upper limit and the kinetic energy above the lower limit are of the same order of magnitude. As a consequence, this wave function has a large overlap with the continuum states, resulting in a strong coupling and thus a large width.

In the simple BO picture of a resonance level, the electronic part of the wave function of a resonance below the $N=2$ threshold (i.e., the dependance on **r**) must be that of a $p\mu(N=2)$ atom in the (quasi) homogeneous electric field of the proton, that is the antisymmetric combination of the $2s_{M=0}$ and $2p_{M=0}$ hydrogenic orbitals around one nucleus, symmetrized with respect to the two nuclei. We denote it

$$\xi(\mathbf{r}) = [\varphi_{as}(\mathbf{r}_1) + \varphi_{as}(\mathbf{r}_2)]/\sqrt{2}, \qquad (8)$$

where

$$\varphi_{as}(\mathbf{r_i}) = [\varphi_{2,0,0}(\mathbf{r_i}) - \varphi_{2,1,0}(\mathbf{r_i})]/\sqrt{2}. \qquad (9)$$

The rotated wave function of a resonance, $|\Psi_v^{0,0}(\theta_S)\rangle$, is a square integrable function. For an isolated resonance close to the real axis, it is related to the unrotated wave function by
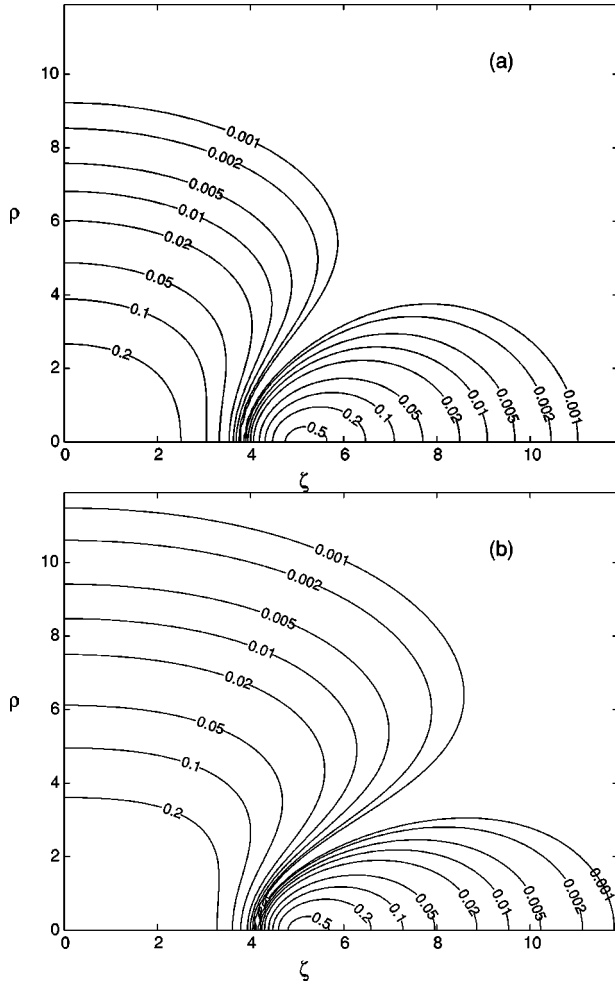
FIG. 4. (a) Contour plot in the (ζ, ρ) plane of the electronic part of the $pp\mu$ $v=0$ resonance below the $N=2$ threshold. (b) Contour plot of the approximate electronic wave function $|\xi|^2$ (see text). ζ and ρ are defined in Fig. 1.

$$|\Psi_v^{0,0}\rangle = R(-\theta_S)|\Psi_v^{0,0}(\theta_S)\rangle, \tag{10}$$

where $R(\theta)$ is the complex rotation operator. The electronic probability density is given by $\text{Re}[\langle \mathbf{r} | \Psi_v^{0,0}(\theta_S)\rangle^2]$. In Fig. 4, the comparison of the wave function of the $v=0$ resonance of $pp\mu$ below the $N=2$ threshold with the predicted wave function $|\xi(\mathbf{r})|^2$ confirms that a resonance state can be seen as a $p\mu$ atom polarized by the field of the second nucleus.

III. RADIATIVE DECAY RATES

A. The decay rate

The $^1S^e$ resonance levels can decay via spontaneous emission since they are coupled to the $^1P^o$ continua by the photon field. This decay channel has three components $M_J=0 \rightarrow M_J=0, \pm 1$. For a symmetric molecule and in the dipole approximation, the coupling operator is

$$\mathbf{d} = qa_0(1+\epsilon)\mathbf{r}, \tag{11}$$

where $\epsilon = 1/(1+2M/m)$. The standard components of $\mathbf{r}$ write

$$r_{M_J} = \mathcal{D}_{M_J 0}^{1^*}(\theta, \psi, \phi)\zeta + \frac{\mathcal{D}_{M_J-1}^{1^*}(\theta, \psi, \phi) - \mathcal{D}_{M_J 1}^{1^*}(\theta, \psi, \phi)}{\sqrt{2}}\rho. \tag{12}$$

From the Fermi golden rule, and summing over all the directions of the emitted photons, we obtain the decay rate per unit photon energy (or x-ray spectrum) for the component $0 \rightarrow M_J$:

$$\frac{d\Gamma_{M_J}}{d(\hbar\omega)} = \frac{q^2}{4\pi\varepsilon_0}\frac{4}{3}(1+\epsilon)^2\frac{(\hbar\omega)^3}{\hbar^4 c^3}a_0^2|\langle\Psi^{1,M_J}(E)|r_{M_J}|\Psi_v^{0,0}\rangle|^2, \tag{13}$$

where $\hbar\omega$ is the photon energy and where $|\Psi^{1,M_J}(E)\rangle$ is the $^1P^o$ continuum state of energy $E=E_s-\hbar\omega$, normalized per unit energy. From the Wigner Eckart theorem, the quantity $\langle\Psi^{1,M_J}|r_{M_J}|\Psi_v^{0,0}\rangle$ does not depend on M_J. Consequently, the total radiative decay rate Γ_γ of the $^1S^e$ resonant state writes

$$\Gamma_\gamma = 3\int_0^\infty \frac{d\Gamma_0}{d(\hbar\omega)}d(\hbar\omega). \tag{14}$$

B. The calculation

The numerical calculation of the square modulus of the matrix element involved in the x-ray spectrum (13) follows the method outlined by Recsigno and McKoy [30]. In that expression, the resonance wave function $|\Psi_v^{0,0}\rangle$ is related to the numerical complex rotated wave function $|\Psi_v^{0,0}(\theta_S)\rangle$ by Eq. (10). It is obtained using optimized variational parameters α_S, β_S, and θ_S. $|\Psi^{1,0}(E)\rangle$ is a continuum level. It has a long range oscillatory behavior completely different from that of the quasibound resonant state. Using the complex rotation method, it appears as a complex continuum eigenfunction of the $^1P^o$ Schrödinger equation. Because of the numerical truncation of the basis, it is well converged for optimized variational parameters α_P, β_P, and θ_P different from those of the resonant level.

Expanding the square modulus involved in Eq. (13), we introduce the projection operator onto the $^1P^o$ subspace of energy E. It can be expressed with the Green function of the rotated Hamiltonian [31] as

$$|\Psi^{1,M_J}(E)\rangle\langle\Psi^{1,M_J}(E)| = \frac{1}{2i\pi}\left(R(-\theta_P)\frac{1}{H(\theta_P)-E}R(\theta_P) - R(\theta_P)\frac{1}{H(-\theta_P)-E}R(-\theta_P)\right). \tag{15}$$

Inserting Eqs. (10) and (15) into Eq. (13), and using the fact that the two terms are complex conjugate, we obtain

$$\frac{d\Gamma_0}{d(\hbar\omega)} = \frac{4}{3}(1+\epsilon)^2\frac{(\hbar\omega)^3}{\hbar^4 c^3}a_0^3\left[-\frac{1}{\pi}\text{Im}(Q_{vv}(E))\right], \quad (16)$$

where $Q_{vv}(E)$ is the dimensionless two-photon transition matrix element we have introduced in [11]. Using the relation $R(\theta)r_z R(-\theta) = e^{i\theta}r_z$, we obtain

$$Q_{vv}(z) = \frac{q^2}{4\pi\varepsilon_0 a_0}\langle\overline{\Psi_v^{0,0}(\theta_S)}|R(\theta_S - \theta_P)$$

$$\times r_z e^{i\theta_P}\frac{1}{z - H_P(\theta_P)}e^{i\theta_P}r_z R(\theta_P - \theta_S)|\Psi_v^{0,0}(\theta_S)\rangle. \quad (17)$$

The expression $\langle\overline{\Psi_v^{0,0}(\theta_S)}|$ means that we only have to transpose $|\Psi_v^{0,0}(\theta_S)\rangle$, without complex conjugation.

C. Numerical calculation

The numerical calculation of the complex matrix element Q_{vv} is very similar to what we have explained in [11]. We only give details on the additional step, applying the complex rotation operator on the resonance wave function. From the numerical point of view, the resonance eigenvectors and the $^1P^o$ Hamiltonian are expanded on two Sturmian bases, defined in Eq. (4), with different variational parameters (α_S, β_S) and (α_P, β_P). We thus have to perform a basis transformation which is simply a dilation by a factor α_P/α_S in the x direction and β_P/β_S in the y and z directions. The dilation operator is

$$\mathcal{D}_x(\alpha_P/\alpha_S)\mathcal{D}_y(\beta_P/\beta_S)\mathcal{D}_z(\beta_P/\beta_S), \quad (18)$$

where $\mathcal{D}_u$ is the dilation operator in the u direction given by

$$\mathcal{D}_u(\delta) = e^{\ln\delta\,(u(\partial/\partial u)+1/2)}. \quad (19)$$

The complex rotation operator $R(\theta)$ in nothing but a dilation by a factor $e^{i\theta}$. Consequently, the basis transformation and the complex rotation can be taken into account into Eq. (17) substituting the complex rotation operator $R(\theta_P - \theta_S)$ by the complex dilation:

$$\mathcal{D}_x\left(\frac{\alpha_P e^{i\theta_P}}{\alpha_S e^{i\theta_S}}\right)\mathcal{D}_y\left(\frac{\beta_P e^{i\theta_P}}{\beta_S e^{i\theta_S}}\right)\mathcal{D}_z\left(\frac{\beta_P e^{i\theta_P}}{\beta_S e^{i\theta_S}}\right). \quad (20)$$

The numerical implementation of this operator is straigthforward since the matrix elements of D_u on the basis functions (5) are known as

$$\langle n|\mathcal{D}_u(e^\gamma)|n'\rangle = (-1)^n\left(\cosh\frac{\gamma}{2}\right)^{-(n+n'+1)}\left(\sinh\frac{\gamma}{2}\right)^{n+n'}$$

$$\times F\left(-n;-n';1;-\frac{1}{\sinh^2\frac{\gamma}{2}}\right), \quad (21)$$

where the hypergeometric function $F(a;b;c;z)$ is a polynomial of degree $\min(n,n')$ [32].

D. Results and discussion

We have computed the x-ray spectrum for the first $^1S^e$ resonances of the different molecular ions below the disso-
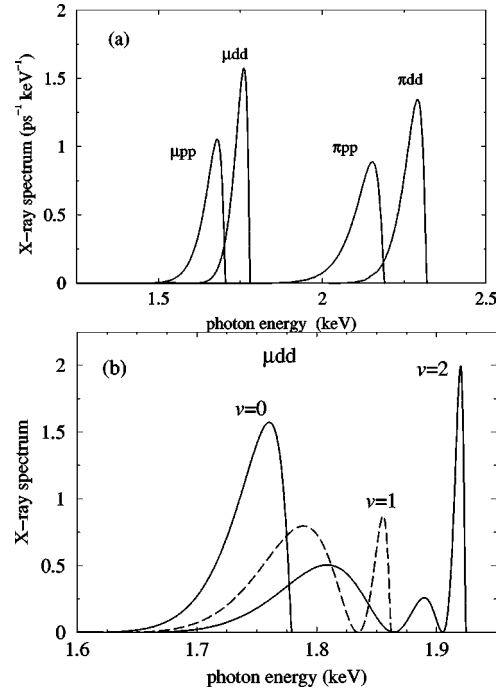
FIG. 5. $^1S^e$ x-ray spectrum of (a) the $v=0$ resonances of the symmetric molecular ions and of (b) the $v=0$, 1, and 2 resonances of $dd\mu$ below the $N=2$ dissociation limit. The x-ray spectra are given by $3[d\Gamma_0/d(\hbar\omega)]$; see Eq. (14). The photon energies corresponding to the maxima of the spectra of $dd\mu$ are, in eV, (1760), (1855,1789) and (1920,1890,1809) for $v=0$, 1 and 2. The corresponding values for $dd\pi$ are (2290), (2427,2332) and (2515,2474,2359).

ciation limit $N=2$. They are plotted in Fig. 5 for the case of $pp\mu$ and $dd\mu$ versus the photon energy. The high energy threshold is determined by the resonance position above the $N=1$ dissociation limit. The shape of the x-ray spectrum is given by Franck-Condon factors that reveal the nodal structure of the wave functions. For low energy photons, the x-ray spectra vanishes because of small Franck-Condon factors and because of the ω^3 factor in Eq. (13).

The radiative decay rates defined by Eq. (14) are obtained by numerical integration of the x-ray spectrum over the photon frequency. The results are given in column 8 of Tables III and IV, with an accuracy 10 times better than those recently published by Lindroth and co-workers [4]. The first comparison of our results to those of Ref. [4] has pointed out a missing mass ratio of about 4 in those results. Our radiative decay rates are now in excellent agreement with the corrected results of Lindroth given in the Erratum [4]. This make us confident on those results.

In Sec. II B 3, we have shown that the electronic part of the wave function of a resonance below the $N=2$ threshold is very close to that of the antisymmetric combination of the $2s$ and $2p$ hydrogenic orbitals. In that picture, the resonance radiative decay rate should be close to half that of the $2p$ level of the atom built with one nucleus (proton or deuteron) and the exotic particle (μ or π). It is given by $\Gamma_{2p} = (2^8/3^8) \times(\tilde{m}e^{10}/\hbar^6 c^3)$ where $\tilde{m}$ is the reduced mass of the light particle. One can observe that the radiative widths of the reso-

TABLE VI. Comparison of the decay rate of the $v=0$ $^1S^e$ resonance of the molecular ions with half the decay rate of the $2p$ level of the corresponding atom.

ion	Γ_γ (ps^{-1})	atom	$\Gamma_{2p}/2$ (ps^{-1})
$pp\mu$	0.0713	$p\mu$	0.0582
$dd\mu$	0.0804	$d\mu$	0.0613
$pp\pi$	0.0879	$p\pi$	0.0745
$dd\pi$	0.1023	$d\pi$	0.0797
$dt\mu$	0.0731	$t\mu$	0.0624

nances of the molecular ions below the $N=2$ threshold we have obtained hardly depend on the vibrational quantum number v. Table VI shows that they compare well with the expected value $\Gamma_{2p}/2$. From the Coulomb and the radiative decay rates Γ_C and Γ_γ, we have computed the branching ratio to the radiative decay channel $\Upsilon_\gamma = \Gamma_\gamma/(\Gamma_C + \Gamma_\gamma)$.

In the case of $pp\mu$, this ratio is of the order of a few percent because the Coulomb decay is much faster than the radiative one. In the case of $dd\mu$ or $dt\mu$, the situation is reversed and the radiative branching ratio is can be as large as 93% for the $v=0$ $^1S^e$ resonance of $dd\mu$. The mean branching ratio to the Coulomb channel is 20% in $dd\mu$ and 96% in $pp\mu$; this result is compatible with the observations of the PSI experiments where the high kinetic energy component is about 4 times smaller for $d\mu$ than for $p\mu$. The formation of $dd\mu^*$ excited molecules during collisions between $d\mu(2s)$ atoms and D_2 should be observable through its x-ray emission spectrum, depicted in Fig. 5. In the caption, we give the photon energies corresponding to the maxima of the emission spectra of the resonances of $dd\mu$ as well as the corresponding ones for $dd\pi$.

The Coulomb and radiative decay rates of the pionic molecules have to be compared to the absorption rate of the pion by the nucleus. An upper bound of the absorption rate Γ_{abs} of a resonance below the N dissociation threshold is given by the absorption rate of the (Ns) state of pionic hydrogen. The measured absorption width of the $p\pi(1s)$ and $d\pi(1s)$ states are 865 and 1020 meV [5,6], corresponding to decay rates of 1314 and 1550 ps^{-1}. Since it is proportional to the s state probability density at the origin, it decreases as $1/N^3$ for excited states. Consequently, the absorption rates of the resonances below the $N=2$, 3, and 4 threshold are expected to be of the order of 164, 50, and 20 ps^{-1} in the case of $pp\pi$, and 194, 57, and 24 ps^{-1} in the case of $dd\pi$.

For the resonances of $pp\pi$ below the $N=2$ dissociation limit, the nuclear absorption rate is much larger than the

Coulomb decay rate. Below the $N=3$ threshold, the two decay rates are comparable, and the Coulomb decay rate becomes the leading one below the $N=4$ threshold. The radiative decay rate that decreases with N remains negligible. As a consequence, high kinetic energy $p\pi$ atoms can be produced by the side path mecanism introduced by Froelich [9] from the resonances below the $N=3$, 4 or higher thresholds. In the case of $dd\pi$, the dominant decay channel remains nuclear absorption for all the $^1S^e$ resonances given here.

IV. CONCLUSION

In this paper, we have presented the calculation of the bound levels and of the $^1S^e$ resonances of muonic or pionic hydrogen molecular ions. The results are obtained by diagonalising the three body Hamiltonian in a complex Sturmian basis. The resonance energies and widths are given with an accuracy in the 10^{-11} a.u. range, improving the accuracy of previously published results. The Coulomb decay rate strongly depends on the nucleus to muon (or pion) mass ratio M/m; for the first $J=0$ resonance of $pp\mu$, this quantity is divided by 444 if the proton is substituted by a deuteron.

We have computed the $^1S^e$ spontaneous emission x-ray spectra and obtained the radiative decay rates of the resonances of the molecular ions. The radiative decay rate only slightly depends on the mass ratio M/m. As a consequence, for the first $J=0$ resonances, the main decay channel is the Coulomb one in the case of $pp\mu$, whereas it is the radiative one in the case of $dd\mu$. This result is consistent with the recent experimental observations.

In the case of $pp\pi$, nuclear absorption is the main decay channel for the $^1S^e$ resonances below the $N=2$ dissociation treshold, whereas Coulomb decay becomes comparable or larger for resonances below higher thresholds. In the case of $dd\pi$, the Coulomb as well as the radiative decay rate remains much smaller than the nuclear absorption one.

[1] R. Pohl, H. Daniel, F. J. Hartmann, P. Hauser, Y. W. Liu, F. Kottmann, C. Maierl, V. E. Markushin, M. Mühlbauer, C. Petitjean, W. Schott, and D. Taqqu, Hyperfine Interact. **138**, 35 (2001).

[2] F. Kottmann, W. Amir, F. Biraben, C. A. N. Conde, S. Dhawan, T. W. Hansch, F. J. Hartmann, V. W. Hughes, O. Huot, P. Indelicato, L. Julien, P. Knowles, S. Kazamias, Y. W. Liu, F. Mulhauser, F. Nez, R. Pohl, P. Rabinowitz, J. M. F. Dos-Santos, L. A. Schaller, H. Schneuwly, W. Schott, D. Taqqu, and J. F. C. A. Veloso, Hyperfine Interact. **138**, 55 (2001)

[3] J. Wallenius, S. Jonsell, Y. Kino, and P. Froelich, Hyperfine Interact. **138**, 285 (2001).

[4] E. Lindroth, J. Wallenius, and S. Jonsell, Phys. Rev. A **68**, 032502 (2003); **69**, 059903 (2003).

[5] D. Chatellard *et al.*, Phys. Rev. Lett. **74**, 4157 (1995).

[6] D. F. Anagnostopoulos *et al.*, Hyperfine Interact. **138**, 131 (2001).

[7] A. Badertscher, M. Daum, R. Frosch, P. F. A. Goudsmit, W. Hajdas, M. Janousch, P.-R. Kettle, V. Markushin, J. Schott-müller, and Z. G. Zhao, Phys. Lett. B **392**, 278 (1997).

[8] S. Jonsell, J. Wallenius, and P. Froelich, Phys. Rev. A **59**, 3440 (1999).

[9] P. Froelich and J. Wallenius, Phys. Rev. Lett. **75**, 2108 (1995).

[10] L. Hilico, N. Billy, B. Grémaud, and D. Delande, Eur. Phys. J. D **12**, 449 (2000).

[11] L. Hilico, N. Billy, B. Grémaud, and D. Delande, J. Phys. B **34**, 491 (2001).

[12] A. S. Coolidge and H. M. James, Phys. Rev. **51**, 855 (1937).

[13] P. J. Mohr and B. N. Taylor, J. Phys. Chem. Ref. Data **28**, 1713 (1999).

[14] E. R. Cohen and B. N. Taylor, Rev. Mod. Phys. **59**, 1121 (1987).

[15] See http://pdg.lbl.gov

[16] D. H. Bailey and A. Frolov, J. Phys. B **35**, 4287 (2002).

[17] V. I. Korobov, Hyperfine Interact. **101/102**, 307 (1996).

[18] J. Ackermann, Phys. Rev. A **57**, 4201 (1990).

[19] A. M. Frolov, Phys. Rev. E **64**, 036704 (2001); J. Phys. B **34**, 3813 (2001).

[20] J. Aguilar and J. M. Combes, Commun. Math. Phys. **22**, 269 (1971); E. Balslev and J. M. Combes, *ibid.* **22**, 280 (1971); Y. K. Ho, Phys. Rep. **99**, 1 (1983).

[21] S. Hara and T. Ishihara, Phys. Rev. A **40**, 4232 (1989).

[22] O. I. Tolstikhin, I. Y. Tolstikhina, and C. Namba, Phys. Rev. A **60**, 4673 (1999).

[23] O. I. Tolstikhin, V. N. Ostrovsky, and H. Nakamura, Phys. Rev. Lett. **79**, 2026 (1997).

[24] G. V. Mil'nikov and H. Nakamura, Phys. Rev. A **67**, 034501 (2003).

[25] J. Wallenius and P. Froelich, Phys. Rev. A **54**, 1171 (1996).

[26] P. M. Morse and H. Feshbach, *Methods of Theoretical Physics* (McGraw-Hill, New York, 1953).

[27] L. Landau and E. Lifchitz, *Quantum Mechanics* (MIR, Moscow, 1966).

[28] L. T. Choo, M. C. Crocker, and J. Nuttall, J. Phys. B **11**, 1313 (1978).

[29] C. Y. Hu and A. K. Bhatia, Phys. Rev. A **43**, 1229 (1991).

[30] T. N. Recsigno and V. McKoy, Phys. Rev. A **12**, 522 (1975).

[31] A. Buchleitner, B. Grémaud, and D. Delande, J. Phys. B **27**, 2663 (1994).

[32] M. Abramovitz and I. A. Stegun, *Handbook of Mathematical Functions* (Dover, New York, 1972).